npj | biological timing and sleep

Article

https://doi.org/10.1038/s44323-025-00023-7

Deletion of *Arntl*, a component of the molecular clock, in adipocytes leads to cellular hypertrophy by increasing insulin sensitivity via FGF21

Hirotake Ishii, Satoshi Kitaura, Taira Wada & Shigeki Shimba ✉

Brain and muscle Arnt-like protein 1 (BMAL1), encoded by *Aryl hydrocarbon receptor nuclear translocator like 1* (*Arntl*) gene, is a transcription factor that regulates the circadian rhythm of the expressions of several genes. The link between the loss of BMAL1 function in adipose tissue and obesity has been reported. Although these previous studies have suggested that dysregulation of lipolysis is a contributing factor, but the detailed mechanism has not been fully understood. This study aimed to elucidate the role of BMAL1 in adipocytes using adipocyte-specific *Arntl* deficient (AAKO) mice. Deletion of *Arntl* in adipocytes leads to increased cellular insulin sensitivity, which in turn, inhibited lipolysis in adipocytes and caused cellular hypertrophy. The expression levels of *Fgf21* in adipose tissue were significantly elevated in AAKO mice compared to *Arntl* $^{flox/flox}$ mice. Double knockout of *Arntl* and *Fgf21* in adipocytes abolished metabolic phenotypes such as decreased circulating non-esterified fatty acid levels, adipocyte hypertrophy, and increased insulin sensitivity in AAKO mice. These results indicated that BMAL1 regulates fat mobilization and insulin signaling in adipocytes via FGF21 during the stationary phase. This is the possible mechanism by which disruption of circadian rhythm induces obesity.

The circadian rhythm of behavior and physiology is produced by the circadian clock system. The circadian clock system is regulated by an autoregulatory network of multiple clock genes at the level of gene expression, translation, and post-translational modifications[1]. In this system, brain and muscle Arnt-like protein 1 (BMAL1 encoded by *Arntl* gene) plays crucial roles as a transcription factor that regulates the circadian rhythm of gene expression[2–7]. BMAL1 forms heterodimers with *circadian locomotor output cycles kaput* (CLOCK), which drives transcription from E-box elements found in the promoters of circadian-regulated genes including *period 1* and *cryptochrome*. Extensive gene expression analysis of mouse livers has revealed the presence of approximately 5900 BMAL1 binding sites in the genome, many of which are related to carbohydrate and lipid metabolism[8,9]. Global *Arntl*$^{-/-}$ mice show several severe phenotypes, including changes in the rhythmicity of behavior, circulating lipid and glucose levels, and ectopic fat formation in the liver and skeletal muscle[10–12]. *Clock* mutant mice are obese and develop metabolic syndromes, characterized by hyperleptinemia, hyperlipidemia, and hyperglycemia[13]. These results indicate that BMAL1 regulates energy metabolism in addition to controlling the circadian rhythm of behavior.

The link between the loss of BMAL1 function in adipose tissue and obesity has been reported. Significant decreases in the expression levels of *Arntl* and its targets have been observed in the adipose tissue of obese humans and mice[14–19]. *ARNTL* methylation is significantly correlated with anthropometric parameters such as body mass index and adiposity[20,21]. In addition, *ARNTL* polymorphisms are significantly associated with central obesity and sex-specific effects on *ARNTL*-mediated genetic susceptibility to obesity[22]. The studies with mice model have suggested that dysregulation of lipolysis in adipose tissue is a contributing factor[23,24]. While several reports have shown a relationship between the loss of BMAL1 functions and obesity as described above, the precise mechanism by which *Arntl* dysfunction leads to obesity has not been fully understood.

Here, we show that the deletion of *Arntl* in adipocytes led to increased cellular insulin sensitivity, which in turn, inhibited lipolysis in adipocytes and caused cellular hypertrophy. The mechanism

Department of Health Science, School of Pharmacy, Nihon University 7-7-1 Narashinodai, Funabashi, Chiba, Japan. ✉e-mail: shimba.shigeki@nihon-u.ac.jp

underlying this increase in insulin sensitivity involves increased FGF21 expression levels in adipocytes. These results indicated that BMAL1 regulates fat mobilization and insulin signaling in adipocytes via FGF21 during the stationary phase.

Results

Deletion of *Arntl* in adipocytes reduced lipid mobilization during the stationary phase

The deletion of *Arntl* gene specifically in adipose tissue of mice was assessed by PCR genotyping of tissues (Supplementary Fig. 1a). *Arntl* gene was deleted in the epididymal white adipose tissue (eWAT) of AAKO mice (homozygous for the Arntl conditional allele (*Arntl* $^{flox/flox}$) carrying the Cre recombinase transgene (*Adipoq-Cre*)). No excised alleles of *Arntl* gene defects were found in the adipose tissue of either mice homozygous for the *Arntl* conditional allele but not carrying Cre recombinase or mice carrying Cre recombinase without the *Arntl* conditional allele. No genetic defects were found in the livers of all types of mice (Supplementary Fig. 1a). The gene expression levels of clock genes and clock-controlled genes in the eWAT of AAKO mice were greatly varied, indicating disruption of clock function (Supplementary Fig. 1b).

We then investigated the respiratory quotient (RQ) to characterize the metabolic activity of AAKO mice. While the RQ values in *Arntl* $^{flox/flox}$ mice displayed a circadian rhythm, those in AAKO mice were almost constant throughout the day and were higher than those in *Arntl* $^{flox/flox}$ mice during the stationary phase (Fig. 1a). In contrast, the food intake level (Fig. 1b), locomotor activity (Fig. 1c), and VO_2 value (Fig. 1d) did not differ between the genotypes (Fig. 1b–d). The higher RQ value in AAKO mice compared to *Arntl* $^{flox/flox}$ mice suggested lower utilization of fat as an energy source in AAKO mice (Fig. 1a). Thus, to confirm this hypothesis, we measured blood biochemical parameters, including non-esterified fatty acids (NEFA), triglyceride (TG), cholesterol, glucose, and leptin levels (Fig. 1e). The results presented in Fig. 1e show that serum NEFA levels were lower in AAKO mice than *Arntl* $^{flox/flox}$ mice at ZT10 (Fig. 1e). Although the eWAT weight per BW did not differ between the genotypes (Fig. 1f), histological analysis showed that adipocytes in the eWAT were larger in AAKO mice than *Arntl* $^{flox/flox}$ mice at ZT10 (Fig. 1g).

Deletion of *Arntl* in adipocytes reduced lipolysis in the eWAT during the stationary phase

The results shown in Fig. 1 indicate that the deletion of the *Arntl* gene in adipocytes decreased the serum levels of NEFA, resulting in an increase in adipocyte size. The expression level of genes related to lipolysis and lipogenesis in the eWAT were not significantly different between the two genotypes (Supplementary Fig. 2). Hormone sensitive lipase (HSL) is an intracellular lipase responsible for releasing NEFA from adipose tissue into the circulation. Phosphorylation at Ser563 and Ser660 activates HSL, whereas phosphorylation at Ser 565 inhibits its activity[25–27]. Deletion of the *Arntl* gene in adipocytes decreased the phosphorylation level of HSL at Ser563 and Ser660 residues in the eWAT (Fig. 2a). In contrast, the phosphorylation level of HSL at Ser565 was higher in the eWAT of AAKO mice than the eWAT of *Arntl* $^{flox/flox}$ mice at ZT10 and 16 (Fig. 2a). However, total HSL levels were not significantly different between the two groups (Fig. 2a). HSL phosphorylation is regulated by the cAMP-PKA pathway. To evaluate the activity of the cAMP-PKA pathway, phosphorylation status of cAMP response element binding protein (CREB) was determined. Deletion of the *Arntl* gene in adipocytes decreased the phosphorylation level of CREB at Ser133 residues in the eWAT (Fig. 2a). Indeed, cAMP level and PKA activity were lower in the eWAT of AAKO mice than the eWAT of *Arntl* $^{flox/flox}$ mice at ZT10 (Fig. 2b, c). Furthermore, the activity of phosphodiesterase (PDE), which is responsible for cAMP degradation, was significantly higher in AAKO mice than *Arntl* $^{flox/flox}$ mice at ZT10 (Fig. 2d).

Deletion of *Arntl* in adipocytes increased insulin sensitivity in the eWAT during the stationary phase

The activity of cAMP-PKA signaling pathway is tightly regulated by insulin[28,29]. The deletion of *Arntl* in adipocytes had no effect on serum insulin levels (Fig. 3a). Therefore, to evaluate insulin sensitivity, the mice were subjected to insulin tolerance test (ITT). The results showed that the insulin-dependent whole-body glucose disposal rate was faster in AAKO mice than in *Arntl* $^{flox/flox}$ mice at ZT10, but not at ZT22 (Fig. 3b).

The glucose uptake rate in tissues was measured using [^{3}H]-2-DG[30]. The results showed that insulin-dependent [^{3}H]-2-DG uptake was higher in the eWAT of AAKO mice than the eWAT of *Arntl* $^{flox/flox}$ mice at ZT10 but not at ZT22 (Fig. 3c). In contrast, the insulin-dependent glucose uptake ratio in the skeletal muscle was comparable between *Arntl* $^{flox/flox}$ and AAKO mice at both ZT10 and ZT 22 (Fig. 3d).

The insulin signal transduction activity in the eWAT was evaluated by determining the phosphorylation level of AKT. The insulin-dependent phosphorylation levels of AKT at Ser473 and Thr308 were higher in the eWAT of AAKO mice than the eWAT of *Arntl* $^{flox/flox}$ mice at ZT10, but not at ZT22 (Fig. 3e). At all times examined, the status of the insulin-dependent phosphorylation of AKT in the skeletal muscle was similar between AAKO mice and *Arntl* $^{flox/flox}$ mice, as was the insulin-dependent glucose uptake (Fig. 3f).

Deletion of *Arntl* increased *Fgf21* gene expression level indirectly via REV-ERBα in adipocytes

Gene expression analysis of the factors associated with insulin sensitivity in the eWAT revealed that the expression levels of *Fgf21* and *β-klotho*, the co-receptor for FGF21, were significantly elevated in AAKO mice compared to *Arntl* $^{flox/flox}$ mice (Fig. 4a, b). The expression of *cFos* and early growth response protein 1 (*Egr1*), representative target genes of FGF21 signaling pathway, was induced in the eWAT by the deletion of *Arntl* (Fig. 4b). An increase in FGF21 protein levels was also observed after the deletion of *Arntl* in the eWAT (Fig. 4c). Serum FGF21 levels were similar between AAKO and *Arntl* $^{flox/flox}$ mice, except at ZT22 (Fig. 4d). *Fgf21* expression in the liver, the major producing organ, was not different between *Arntl* $^{flox/flox}$ mice and AAKO mice (Fig. 4e). The upregulation of *Fgf21* expression in the absence of *Arntl* suggested that *Fgf21* gene expression may be under the negative control of BMAL1, presumably via the reverse orientation the *c-erbA-1* gene (REV-ERBα), a transcriptional suppressor encoded by *Nr1d1* gene[31,32]. *c-erbA-1* is the thyroid hormone receptor alpha gene (*Thra*). *Nr1d1* gene is transcribed from the opposite strand of the *c-erbAα* so that *Nr1d1* and *Thra* are complementary on 269 bases[33,34]. Therefore, we used an siRNA to knockdown the expression of *Nr1d1* in cultured 3T3-L1 adipocytes to determine whether *Fgf21* expression is also regulated by REV-ERBα in adipocytes. The results shown in Fig. 4f indicated that the downregulation of *Nr1d1* expression increased *Fgf21* expression levels (Fig. 4f). E4BP4 (encoded by *Nfil3*) and RORα (encoded by *Rora*) are known to regulate *Fgf21* expression[35,36]. The downregulation of *Nr1d1* expression had no effects on the expression of these factors (Fig. 4f). Overexpression of *Arntl* in the cultured adipocytes also decreased *Fgf21* expression levels, but this effect was counteracted by the knockdown of *Nr1d1* expression in the cells (Fig. 4g). These results indicate that BMAL1 regulates *Fgf21* expression via REV-ERBα. Inspection of *Fgf21* promoter region revealed two putative retinoic acid receptor-related orphan receptor-responsive elements (ROREs) at positions −93 and −60, upstream of the transcription start site (Fig. 4h). Previous studies have shown that *Fgf21* is regulated by REV-ERBα in the liver[37,38]. Recruitment of REV-ERBα to *Fgf21*/RORE in the genome was confirmed using a chromatin immunoprecipitation (ChIP) assay. In this ChIP assay, the mouse *Arntl* promoter region containing an RORE and part of the mouse *Fgf21* gene, which lacks an RORE, were used as positive and negative controls, respectively. As shown in Fig. 4h, time-dependent recruitment of REV-ERBα to the promoter region encompassing *Fgf21*/RORE was observed in the eWAT of *Arntl* $^{flox/flox}$ mice but not AAKO mice (Fig. 4h).

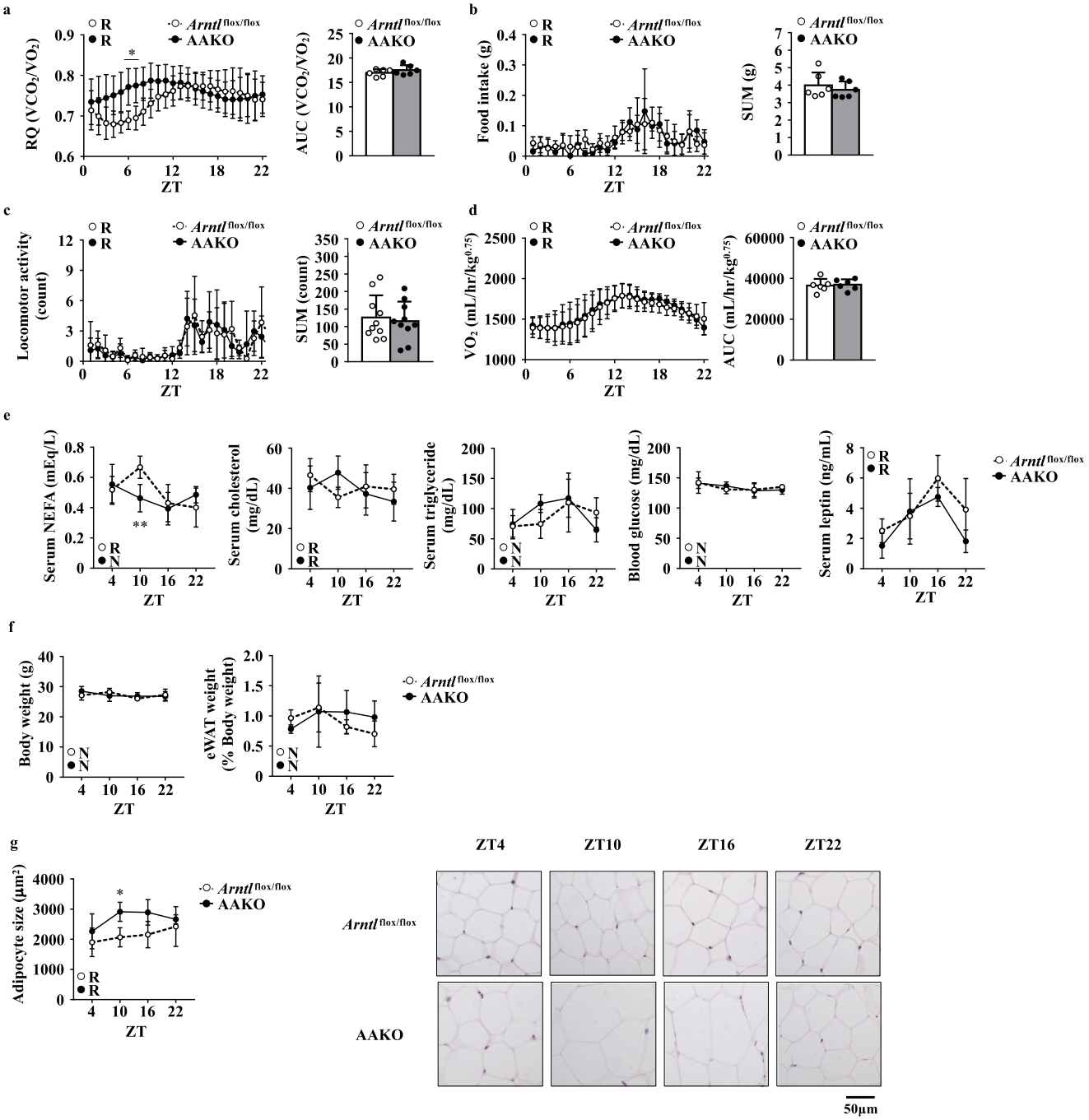

Fig. 1 | Deletion of *Arntl* in adipocytes reduced lipid mobilization during the stationary phase. a–d Metabolic activity of *Arntl1*$^{flox/flox}$ and adipocyte-specific *Arntl1*-knockout (AAKO) mice under a 12-h light-dark cycles . **a** Left, respiratory quotient (RQ) ($n = 6$). Right, the area under the curve (AUC) was calculated for respective group. **b** Left, food intake. Right, the sum of food intake for 24 h was calculated for respective group ($n = 6$). **c** Left, locomotor activity ($n = 10$). Right, the sum of locomotor activity for 24 h was calculated for respective group. **d** Left, oxygen consumption (VO_2). Right, the AUC was calculated for respective group ($n = 6$). **e** Serum non-esterified fatty acid (NEFA), cholesterol, triglyceride, blood glucose, and leptin levels in mice ($n = 4–5$). **f** Left, body weight (BW). Right, the epididymal white adipose tissue (eWAT) weight relative to BW. **g** Left, quantification of adipocyte size in the eWAT. Right, representative image of hematoxylin and eosin (H&E) staining of the eWAT (right). Data are presented as the mean ± standard deviation (SD) and compared using two-way analysis of variance (ANOVA) with Bonferroni's post-hoc test. $^*P < 0.05$, $^{**}P < 0.01$ relative to the *Arntl*$^{flox/flox}$ mice at the same timepoint. Rhythmicity was calculated using CircWave software. R, rhythmic expression ($P < 0.05$); N, non-rhythmic expression ($P > 0.05$).

Deletion of *Fgf21* in adipocytes abolished the metabolic phenotype in AAKO mice

To confirm whether the metabolic phenotypes of AAKO mice were due to local increase in FGF21 levels, we generated and analyzed the adipocyte-specific *Arntl* and *Fgf21* double knockout mice (AdKO mice). The increased RQ values, decreased serum NEFA level, and adipocyte hypertrophy observed in the AAKO mice were not observed in AdKO mice (Fig. 5a–c). No differences in food intake level, locomotor activity, VO_2 value, BW, or adipose tissue weight per BW were observed between the *Arntl*$^{flox/flox}$*Fgf21*$^{flox/flox}$ mice and the AdKO mice, as there were no differences between the *Arntl* $^{flox/flox}$ mice and the AAKO mice (Fig. 5d–g).

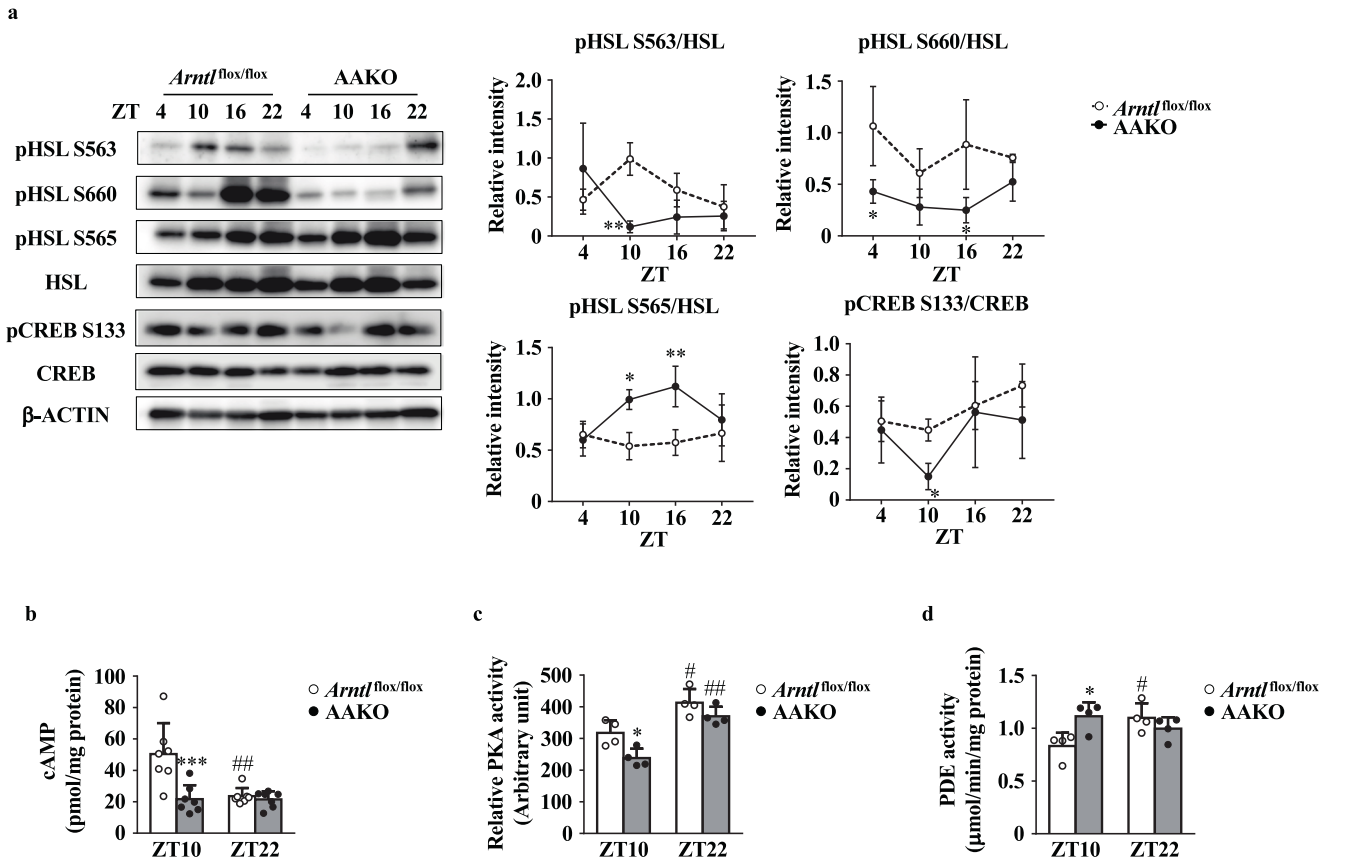

Fig. 2 | Deletion of *Arntl* in adipocytes reduced lipolysis. a Left, representative western blot of total hormone-sensitive lipase (HSL), phosphorylated HSL, total cAMP response element binding protein (CREB), and phosphorylated CREB in the eWAT. β-ACTIN was used as loading control. Right, the relative intensities of the bands were analyzed using Amersham ImageQuant TL ($n = 3$). **b** cAMP levels ($n = 7$). **c** PKA activity ($n = 4$). **d** Phosphodiesterase (PDE) activity ($n = 4$). Data are represented as the means ± SD and were compared using two-way ANOVA with Bonferroni's post-hoc test (**a**) or Tukey's post-hoc test (**b**–**d**). $^{*}P < 0.05$, $^{**}P < 0.01$, $^{***}P < 0.001$, relative to $Arntl^{flox/flox}$ mice at the same timepoint and $^{\#}P < 0.05$, or $^{\#\#}P < 0.01$ relative to ZT10 in the same genotype.

The ITT score of AdKO mice was equal to that of $Arntl^{flox/flox}Fgf21^{flox/flox}$ mice (Fig. 6a). In addition, insulin-dependent [^{3}H]-2-DG uptake in the eWAT was similar between AdKO mice and $Arntl^{flox/flox}Fgf21^{flox/flox}$ mice (Fig. 6b). Furthermore, there were no significant differences in the insulin-dependent phosphorylation level of AKT in the between $Arntl^{flox/flox}Fgf21^{flox/flox}$ mice and AdKO mice (Fig. 6c). Serum insulin level in AdKO mice was comparable to that in $Arntl^{flox/flox}Fgf21^{flox/flox}$ mice (Fig. 6d). Also, the *Fgf21* expression in the liver was not different between $Arntl^{flox/flox}Fgf21^{flox/flox}$ mice and AdKO mice (Fig. 6e).

Discussion

This study aimed to understand the role of *Arntl* in adipose tissue. AAKO mice were used to demonstrate that loss of *Arntl* leads to adipocyte hypertrophy and a decrease in serum NEFA levels (Fig. 1e, g). These phenotypes were attributed to the lower lipolytic activity of the AAKO mice for several reasons. The studies using *Clock* mutant mice and global *Arntl* KO mice proposed that the loss of circadian expression of *Hsl* and *Atgl* results in adipocyte hypertrophy and reduced circulating NEFA levels[23]. The results in the current study showed that the HSL activation pathway signal in the eWAT was significantly weaker in AAKO mice than $Arntl^{flox/flox}$ mice (Fig. 2a–d). Because the HSL activation pathway in the eWAT is tightly regulated by insulin[39–42], changes in insulin levels and/or sensitivity were responsible for the reduction in lipolytic activity in the eWAT of AAKO mice. In support of this, insulin sensitivity increased in the eWAT of the AAKO mice, whereas circulating insulin levels were similar between AAKO mice and $Arntl^{flox/flox}$ mice (Fig. 3a, c, e). Importantly, insulin sensitivity in the skeletal muscle was similar between AAKO mice and $Arntl^{flox/flox}$ mice (Fig. 3d, f). Increased lipogenesis and fatty acid uptake may also induce adipocyte hypertrophy. However, the expressions levels of genes related to lipogenesis, fatty acid uptake, and acetyl-CoA carboxylase (ACC) phosphorylation status in the eWAT were similar between AAKO mice and $Arntl^{flox/flox}$ mice (Supplementary Fig. 2). Therefore, we conclude that the increase in local insulin sensitivity in the eWAT and the subsequent reduction in lipolytic activity induced adipocyte hypertrophy and decreased circulating NEFA levels in AAKO mice.

Together with increased local insulin sensitivity, one of the most notable changes in the eWAT of AAKO mice was the induction of *Fgf21* expression (Fig. 4a). FGF21, a cytokine secreted by various tissues including adipose tissue, increases insulin sensitivity in adipose tissue[30]. Most of the FGF21 produced in the liver is secreted into the circulation. In contrast, FGF21 produced in the adipose tissue is not secreted into the bloodstream and acts only on adipose tissue[43,44]. Therefore, the increase in local insulin sensitivity in the eWAT of AAKO mice can be attributed to a higher level of *Fgf21* expression in the eWAT. Indeed, FGF21 target genes, including *cFos* and *Egr1*, were superinduced in the eWAT (Fig. 4b). To confirm the effects of locally produced FGF21, we demonstrated that the double knockout of *Arntl* and *Fgf21* in adipocytes abolished phenotypes such as increased RQ, decreased circulating NEFA level, adipocyte hypertrophy, and increased insulin sensitivity in AAKO mice (Figs. 5, 6). It is well known that BMAL1 downregulates the transcription of *Fgf21* by inducing REV-ERBα, a transcriptional suppressor in the liver[38]. Here we showed that this indirect transcriptional regulation of *Fgf21* by BMAL1 also occurs in adipocytes (Fig. 4f–h). Retinoid-related orphan receptor alpha (RORα) antagonizes REV-ERBα on the RORE sequence[45] and regulates *Fgf21* expression in the liver[36]. However, the expression level of *Rora* in the eWAT was similar

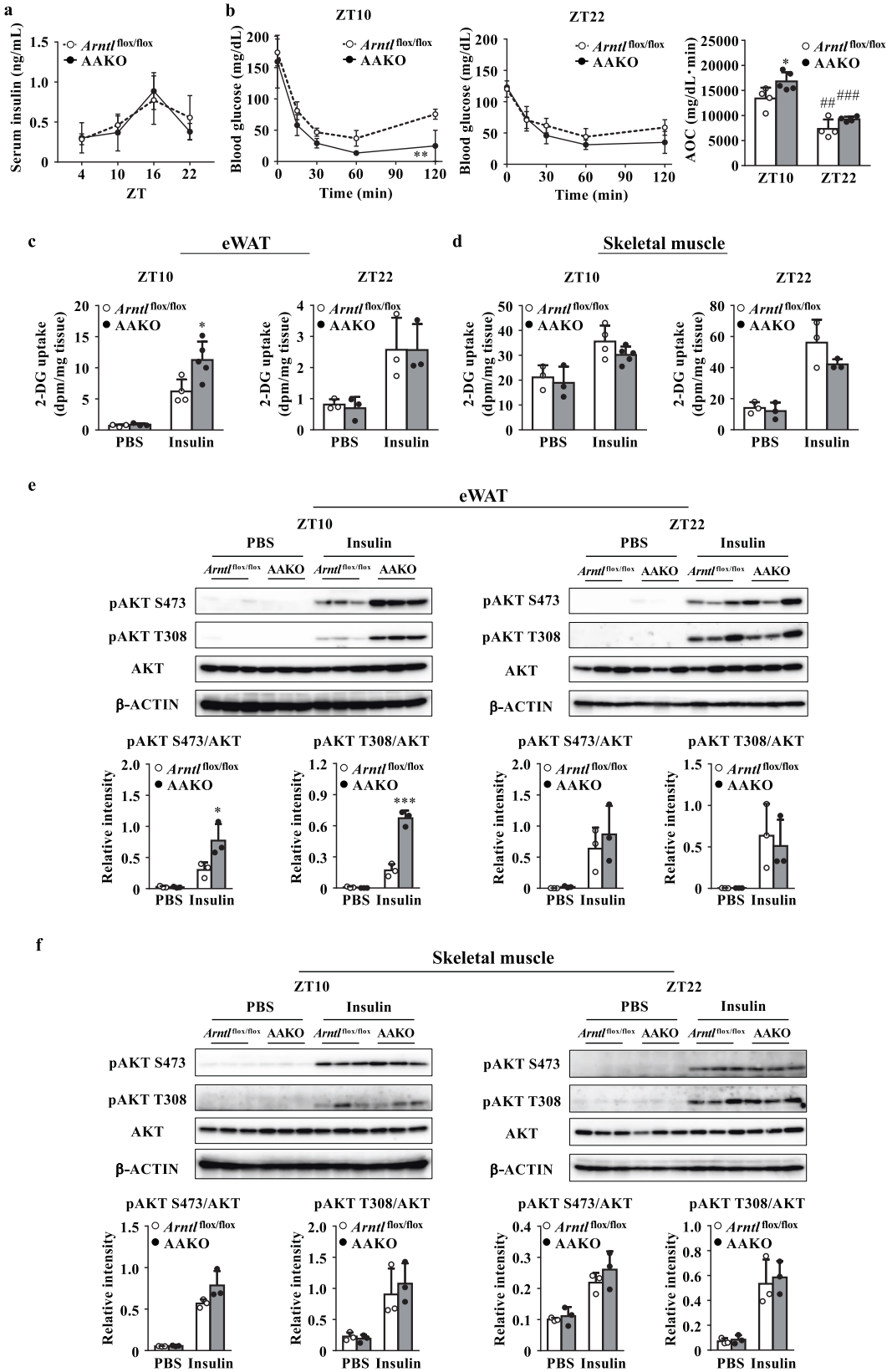

Fig. 3 | Deletion of *Arntl* in adipocytes increased insulin sensitivity in the eWAT. **a** Serum insulin levels in mice ($n = 3$–5). **b** Blood glucose levels during the insulin tolerance test (ITT) at ZT10 and ZT22 and the area over the curve (AOC) was calculated for respective group (right, $n = 4$–5). **c**,**d** [^{3}H]-2-deoxyglucose (2-DG) uptake rate in tissue at ZT10 (left) and ZT22 (right). **c** eWAT. **d** Skeletal muscle. **e**,**f** Top, representative western blot of total AKT and phosphorylated AKT at ZT10 and ZT22. β-ACTIN was used as a loading control. Bottom, the relative intensities of the bands were analyzed using Amersham ImageQuant TL ($n = 3$). **e** eWAT. **f** Skeletal muscle. Data are presented as the mean ± SD and were compared using two-way ANOVA with Bonferroni's post-hoc test (**a**,**b** left and center) or Tukey's post-hoc test (**b** right, **c**–**f**). $^*P < 0.05$, $^{**}P < 0.01$, $^{***}P < 0.001$ relative to *Arntl*$^{flox/flox}$ mice at the same timepoint or treatment and $^{\#\#}P < 0.01$, or $^{\#\#\#}P < 0.001$ relative to ZT10 in the same genotype.

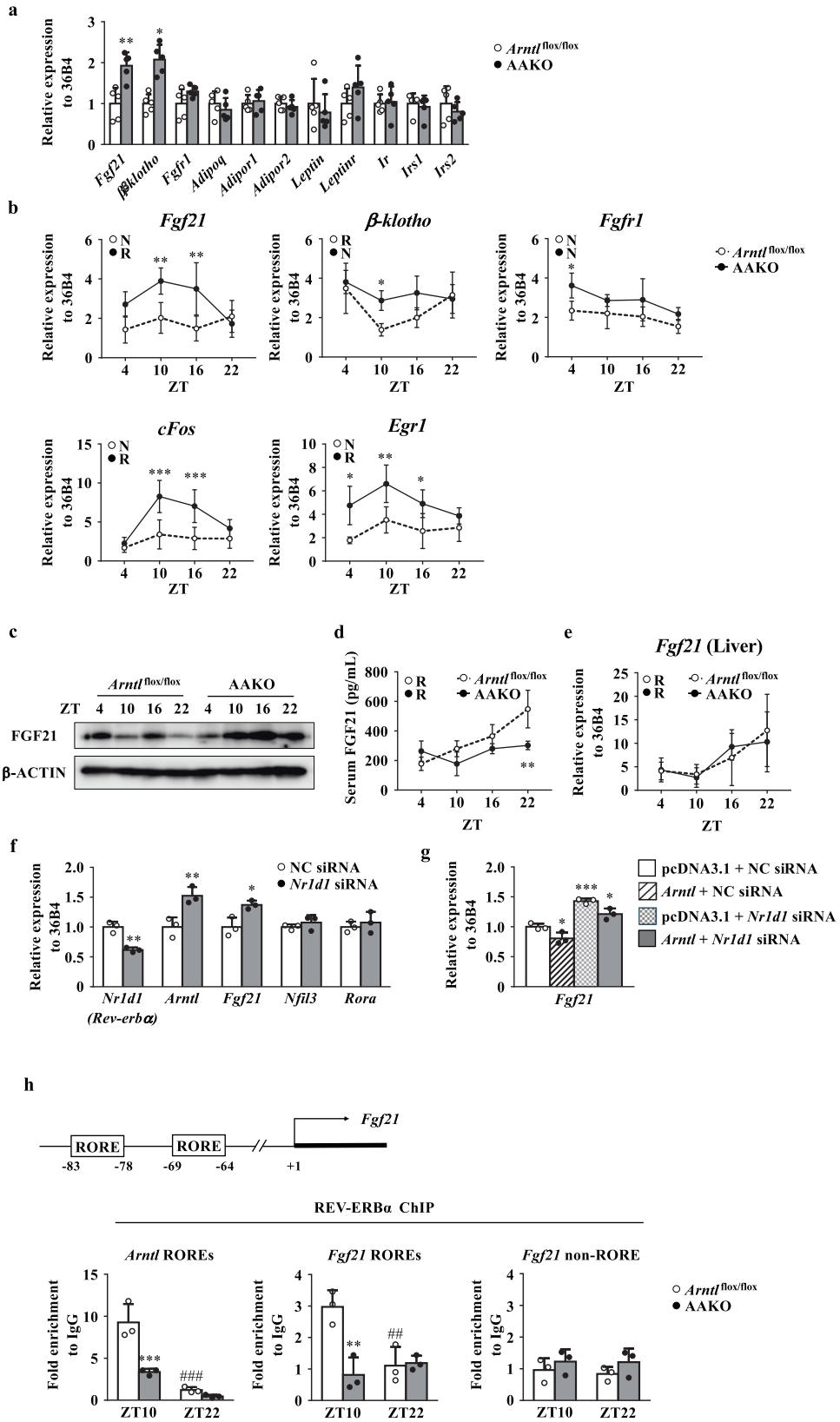

Fig. 4 | Deletion of *Arntl* increased *Fgf21* expression levels indirectly via REV-ERBα in adipocytes. **a** Expression level of genes related to insulin sensitivity in the eWAT of *Arntl*$^{flox/flox}$ and AAKO mice at ZT10 ($n = 5$). **b** Circadian gene expression levels in the eWAT of *Arntl*$^{flox/flox}$ and AAKO mice ($n = 3–5$). **c** Representative western blot of FGF21 in the eWAT. β-ACTIN was used as a loading control. **d** Serum FGF21 levels in *Arntl*$^{flox/flox}$ and AAKO mice ($n = 3–5$). **e** Circadian gene expression levels of *Fgf21* in the liver of *Arntl* $^{flox/flox}$ and AAKO mice ($n = 3$). **f** Gene expression levels of *Nr1d1*, *Arntl*, *Fgf21*, *Nfil3,* and *Rora* in negative control (NC) siRNA- or *Nr1d1* specific siRNA-transfected 3T3-L1 adipocytes. **g** Gene expression levels of *Fgf21* in NC siRNA- or *Nr1d1* specific siRNA-and pcDNA3.1 empty or *Arntl* expression vector transfected 3T3-L1 adipocytes. **h** Top, schematic representation of the mouse *Fgf21* promoter region. Bottom, chromatin immunoprecipitation (ChIP)–quantitative polymerase chain reaction (qPCR) analysis of the interaction between REV-ERBα and the retinoic-acid-receptor-related orphan-receptor-responsive element (RORE) in the mouse *Fgf21* promoter region in the eWAT at ZT10 and ZT22 (bottom. $n = 3$). Non-immune IgG sample was used to normalize the qPCR results in each ChIP sample. The *Arntl* RORE region and *Fgf21* non-RORE region were used as the positive and negative control, respectively. Data are presented as the mean ± SD. Data in (**a**, **f**) were compared using an unpaired Student's t-test with Welch's correction. $^{*}P < 0.05$, $^{**}P < 0.01$ relative to *Arntl*$^{flox/flox}$ mice (**a**) or NC siRNA-transfected 3T3-L1 adipocytes (**f**). Data in panels were compared using two-way ANOVA with Bonferroni's (**b**,**d**,**e**) or Tukey's (**g**,**h**) post-hoc test. $^{*}P < 0.05$, $^{**}P < 0.01$, $^{***}P < 0.001$ relative to *Arntl*$^{flox/flox}$ mice at the same timepoint (**b**,**d**,**e**,**h**) or NC siRNA- and pcDNA3.1 empty vector transfected 3T3-L1 adipocytes (**g**), $^{\#\#}P < 0.01$, $^{\#\#\#}P < 0.001$ relative to ZT10 for the same genotype (**h**). Rhythmicity was calculated using CircWave software. R, rhythmic expression ($P < 0.05$); N non-rhythmic expression ($P > 0.05$).

between AAKO mice and *Arntl*$^{flox/flox}$ mice (Supplementary Fig. 1b). Therefore, the increased gene expression levels of *Fgf21* in the eWAT of AAKO mice was not due to increased expression levels of RORα but was associated with reduced expression levels of REV-ERBα and the consequent relative dominance of other positive transcriptional regulators, including RORα. E4BP4 strongly suppresses *Fgf21* transcription by binding to a D-box element in the distal promoter region in the liver[35]. In the present study, deletion of *Arntl* increased the expression level of both *Nfil3* (E4BP4) and *Fgf21* in the eWAT (Supplementary Fig. 1b). Knockdown of *Nr1d1* increased the *Fgf21* expression but had no effects on the expression of *Nfil3*

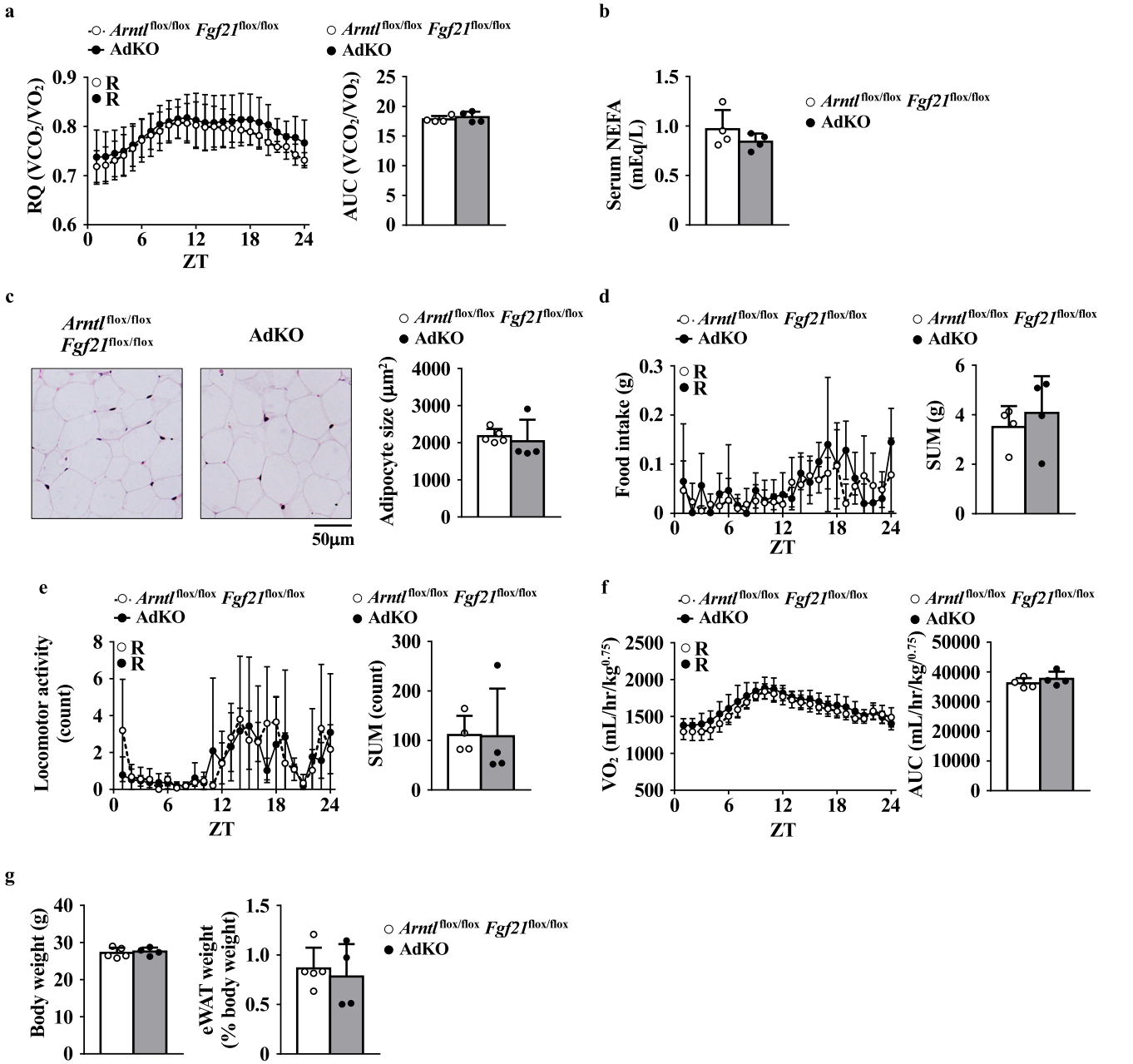

Fig. 5 | Deletion of *Fgf21* in adipocytes abolished the metabolic phenotype in AAKO mice. a Left, RQ. Right, the AUC was calculated for respective group ($n = 4$). **b** Serum NEFA levels in mice at ZT10 ($n = 4$). **c** Left, representative image of H&E staining of the eWAT. Right, quantification of adipocyte size in the eWAT at ZT10 ($n = 4$–5). **d** Left, food intake. Right, the sum of food intake for 24 h was calculated for respective group ($n = 4$). **e** Left, locomotor activity. Right, the sum of locomotor activity for 24 h was calculated for respective group ($n = 4$). **f** Left, VO_2. Right, the AUC was calculated for respective group ($n = 4$). **g** Left, BW. Right, relative the eWAT weight per BW at ZT10 ($n = 4$–5). Metabolic activity of the *Arntl*$^{flox/flox}$ *Fgf21*$^{flox/flox}$ and the adipocyte-specific *Arntl* and *Fgf21* double-knockout (AdKO) mice under a 12-hour light-dark cycles. Data are presented as the mean ± SD (**a**, **d**–**f** left) and were compared using two-way ANOVA with Bonferroni's post-hoc test. Data in panels were compared using an unpaired Student's t-test with Welch's correction (**a**–**f** right, **g**). Rhythmicity was calculated using CircWave software. R, rhythmic expression ($P < 0.05$); N non-rhythmic expression ($P > 0.05$).

in 3T3-L1 adipocytes (Fig. 4f). These results indicated that E4BP4 is not involved in the induction of *Fgf21* expression in the eWAT of AAKO mice. Taking these results together, we conclude that BMAL1 plays a role in regulating insulin sensitivity and the consequent release of fatty acids, which are a major source of energy during quiescence, via indirect regulation of FGF21 expression by REV-ERBα in adipocytes.

Decreased circulating NEFA levels and adipocyte hypertrophy in mice due to the deletion of *Arntl* in adipocytes have also been reported by Paschos et al.[24]. The proposed mechanism is that the disruption of the adipocyte clock function results in temporal changes in the plasma concentration of polyunsaturated fatty acids, leading to corresponding changes in the expression of neurotransmitters responsible for appetite regulation in hypothalamic feeding centers. Therefore, mice lacking *Arntl* in adipocytes exhibit excessive food intake[24]. Also, the increased circulating leptin level was observed in the previous model[24,46]. However, in our study, the food intake level and the associated behavior were similar in AAKO mice and *Arntl*$^{flox/flox}$ mice (Fig. 1b). The level of circulating leptin and *leptin* gene expression in adipose tissue of AAKO mice was comparable to those of

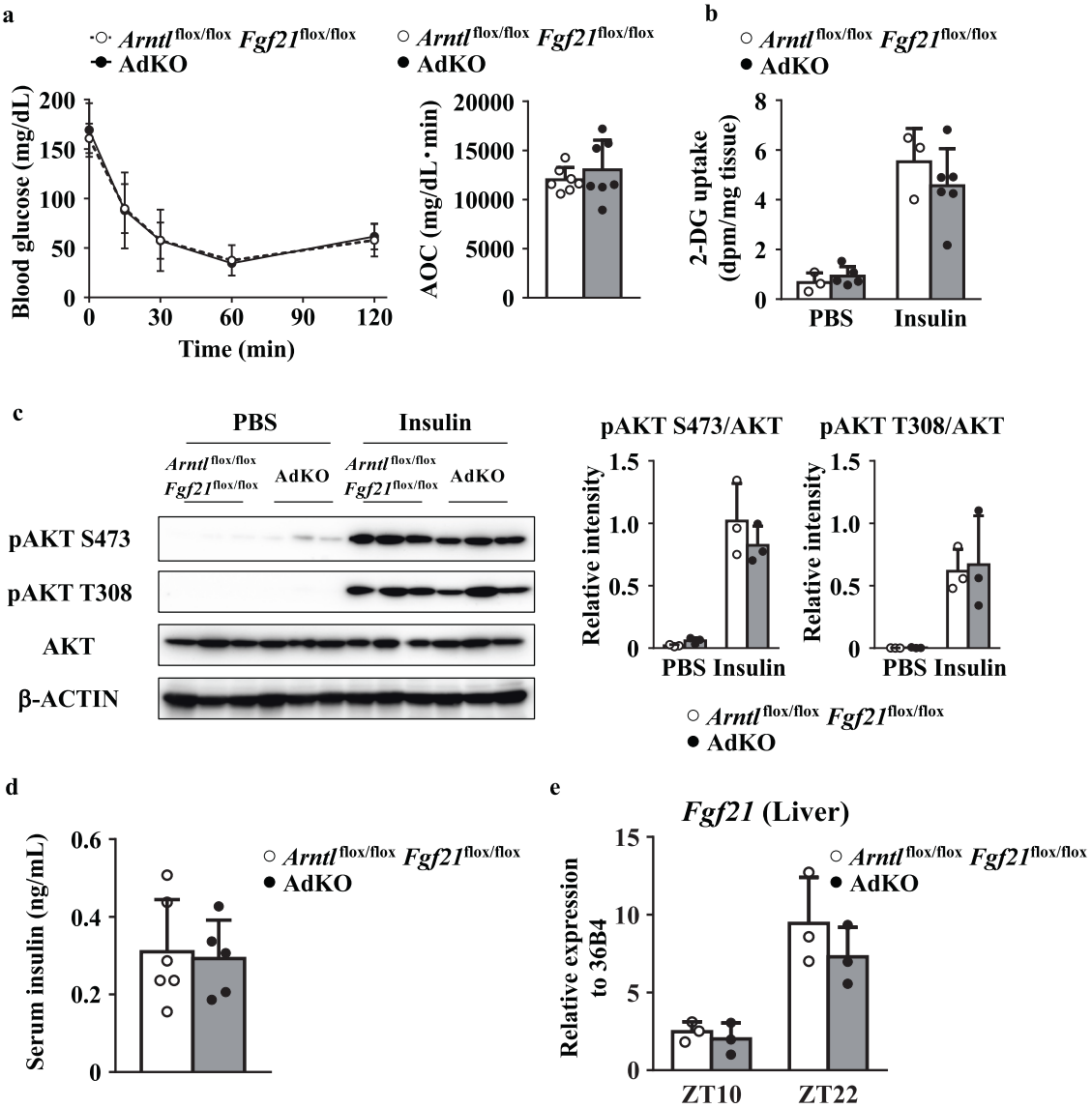

Fig. 6 | Deletion of *Fgf21* in adipocytes abolishes the increased insulin sensitivity in the eWAT of AAKO mice. a Left, blood glucose levels in mice during the ITT at ZT10. Right, the AOC was calculated for respective group ($n = 7$). **b** Glucose uptake rate in the eWAT at ZT10 ($n = 3$–6). **c** Left, representative western blot of total AKT and phosphorylated AKT in the eWAT at ZT10. Right, the relative intensity of the bands. ($n = 3$). **d** Serum insulin levels in mice ($n = 5$). **e** Circadian gene expression level of *Fgf21* in the liver ($n = 3$). Data are presented as the mean ± SD. Data in panels were compared using two-way ANOVA with Bonferroni's (**a** left) or Tukey's (**b**,**c**,**e**) post-hoc test. Data in panels (**a** right,**d**) were compared using an unpaired Student's *t*test with Welch's correction. β-ACTIN was used as a loading control.

Arntl$^{flox/flox}$ mice (Fig. 1e and Supplementary Fig. 1b). The difference between our study and the above-mentioned study is that mice carrying Cre recombinase to establish adipocyte-specific *Arntl* mice. The previous study has used *aP2* (*Fabp4*)-Cre mice. Several recent studies have shown that the *aP2* (*Fabp4*) promoter is active not only in the adipose tissue but also in various other tissues including the hypothalamus[47–50]. Therefore, the mice generated using the *aP2* (*Fabp4*)-Cre mice showed the change in food intake activity[50]. In the present study, the AAKO mice were generated by crossing *Arntl*$^{flox/flox}$ mice with the mice carrying the Cre recombinase gene driven by the adiponectin promoter. It has been reported that Cre expression driven by the adiponectin promoter leads to recombination that exclusively affects adipocytes[51,52]. The precise cause of the phenotypic differences between the two mouse models is unclear; however, we would like to emphasize that the loss of *Arntl* in adipocytes disrupts lipolysis and leads to cell hypertrophy, a common phenotype in both reports, and that the present study demonstrates a novel mechanism that generates these phenotypes.

Our results showed that the deletion of *Arntl* increased insulin signaling via the regulation of FGF21 expression in the eWAT of mice (Figs. 3, 4). Several reports showed that regulation of insulin sensitivity and insulin signaling by BMAL1 using tissue specific *Arntl* knockout mice. Deletion of *Arntl* in hepatocytes decreases insulin signaling activity and insulin sensitivity in the liver of the mice[53,54]. Hepatic BMAL1 binds to the promoter region of *Sirt1*, which encodes an NAD^+-dependent histone deacetylase, to increase its expression level and regulate hepatic insulin sensitivity[53]. However, the expression level of *Sirt1* in adipocytes was similar between AAKO mice and *Arntl*$^{flox/flox}$ mice (Supplementary Fig. 1b). Therefore, the BMAL1-SIRT1 axis may not be responsible for the increased insulin signaling activity in the eWAT of AAKO mice. While deletion of *Arntl* in the liver increased *Fgf21* expression levels, insulin signaling in the liver was reduced (Supplementary Fig. 3)[53,54]. These results suggest that the BMAL1-FGF21 axis is a major pathway involved in the regulation of insulin signaling in adipocytes but not in hepatocytes in mice. The differences in the effects of *Arntl* deletion on insulin sensitivity between adipose tissue and the liver are partly accounted for the tissue specificity of *Klb* (β-*klotho*) expression[55]. Reduction of *Nr1d1*(REV-ERBα) expression induces *Klb* expression in adipose tissue but not the liver[55]. Since β−Klotho is an

essential coreceptor for FGF21, downregulation of *Nr1d1* (REV-ERBα) expression strongly activates FGF21 signaling and insulin sensitivity in adipose tissue. The induction of *Klb* expression and the activation of FGF21/Klotho signaling pathway were observed in the eWAT of AAKO mice (Fig. 4b and Supplementary Fig. 1b). Therefore, it can be concluded that BMAL1- REV-ERBα -FGF21 axis regulates insulin signaling in a tissue-specific manner.

In conclusion, disruptions of the circadian clock due to an irregular lifestyle such as shift work and a high-fat diet may impair fat mobilization and cause lipid accumulation in adipocytes, which may increase the risk of obesity and related diseases. Our present findings demonstrate the regulation of fat mobilization and insulin signaling by BMAL1 in adipocytes and this is the possible mechanism by which downregulation of *Arntl* and its targets induces obesity[14–19]. Also, since the activity of BMAL1 peaks during the stationary phase[12], the regulation of fat mobilization by BMAL1 may be the mechanism by which fatty acids are used as an energy source during the stationary phase. Therefore, the results in this study also provide additional insight into by which the molecular circadian clock in adipocytes modulates whole-body energy metabolism.

Methods

Animal studies

Conditional *Arntl*$^{flox/flox}$ mice[12], which carry the conditional *Arntl* allele containing exons 6 to 8 flanked by *loxP* sites, were crossed with mice carrying the Cre recombinase gene driven by the adiponectin promoter (The Jackson Laboratory, Bar Harbor, ME, USA). Mice homozygous for the floxed allele and hemizygous for the Cre transgene (adipocyte-specific *Arntl* knockout, AAKO) were obtained by crossing *Arntl*$^{flox/-}$/Cre^{Adipoq} mice with *Arntl*$^{flox/flox}$ mice. Splicing of exons 6 to 8 should cause a deletion of the bHLH domain and a frameshift mutation with the introduction of an early stop codon (TGA)[12]. Genotyping was performed by PCR on DNA isolated from tail biopsies. The *Arntl*-excised allele was amplified by using primer A (5′-GGGGATTTCCATCTGTGTTTAC-3′) and primer B (5′- CTCATCT GCTTATCTGCTCTGGGG -3′). The conditional allele was amplified by using primer B and primer C (5′-TCAACGTTTCGATGCTCGTG-3′). Littermates that were negative for Cre transgenes (*Arntl*$^{flox/flox}$) were used as experimental controls. *Arntl*$^{flox/flox}$ *Fgf21*$^{flox/flox}$ mice were generated by breeding *Arntl*$^{flox/flox}$ mice with *Fgf21*$^{flox/flox}$ mice (The Jackson Laboratory). *Arntl*$^{flox/flox}$ *Fgf21*$^{flox/flox}$ mice were used to generate adipocyte-specific *Arntl* and *Fgf21* double-knockout mice (AdKO mice) in the same manner as described above. All animals were maintained in groups of 3 to 5 animals per cage under a 12-h light-dark cycle at 23 ± 1 °C and 50 ± 10% relative humidity. Food and water were provided *ad libitum*. Male mice (16 to 20 weeks old) were randomly grouped by cage and used in the experiment without any exclusion. All experimental mice were euthanized with carbon dioxide. The experimental methods and design adhered to the ARRIVE guidelines. The experimental protocol was approved by the Ethics Review Committee for Animal Experimentation of Nihon University (approval no. AP17P030) and was executed according to the relevant guidelines and regulations.

Metabolic studies

Mice were individually caged and acclimated for 2 days before measurements were performed. Daily food consumption, oxygen consumption, carbon dioxide production, and respiratory quotients were determined using the Oxylet Pro System (PANLAB, S.L.U. Barcelona, Spain).

Biochemical analysis

The levels of triglyceride (TG), total cholesterol (EKF Diagnostics-Stanbio Laboratory, Boerne, TX, USA), non-esterified fatty acids (NEFA) (Fujifilm Wako Pure Chemical Co. Ltd., Osaka, Japan), insulin, leptin (Morinaga Institute of Biological Science, Inc., Kanagawa, Japan), FGF21(R&D Systems, Minneapolis, MN, USA), and cAMP (Enzo Life Sciences, Farmingdale, NY, USA) were determined using commercial assay kits according to the manufacturer's instructions.

Histological analysis

For histological analysis, the epididymal white adipose tissue (eWAT) was fixed in 10% formaldehyde, embedded in paraffin, sectioned at 5 μm, and stained with hematoxylin and eosin (H&E). The adipocyte area was measured for 50 adipocytes in each sample using cellSens imaging software (Evident Co., Tokyo, Japan).

Preparation of tissue extract

Tissue samples were added to a buffer (50 mM Tris-HCl [pH 8.0], 150 mM NaCl, 0.1% SDS, 1% NP-40, and 0.5% sodium deoxycholate) containing a protease inhibitor cocktail (Fujifilm Wako Pure Chemical) and a phosphatase inhibitor (Roche Diagnostics K. K., Tokyo, Japan) and homogenized using a Dounce grinder. After centrifugation for 10 min at 15,000 *g*, the resulting supernatant was desalted using Zeba Spin Desalting Columns (Thermo Fisher Scientific, Waltham, MA, USA) and assayed.

Western blotting

Proteins were resolved using sodium dodecyl sulfate-polyacrylamide gel electrophoresis (SDS-PAGE), transferred onto the membranes, and probed with relevant antibodies. Immunoreactive proteins were visualized using enhanced chemiluminescence detection reagents from Thermo Fisher Scientific and Cytiva (Marlborough, MA, USA). Images were cropped and adjusted for brightness and contrast. Uncropped and unprocessed images are shown in Supplementary Figs.4–8. Band intensity in uncropped and unprocessed images was quantified using Amersham ImageQuant TL (Cytiva). The anti-hormone sensitive lipase (HSL) antibody was purchased from Santa Cruz Biotechnology, Inc. (Dallas, TX, USA) and anti-phosphorylated HSL anti-cAMP response element binding protein (CREB), anti-phosphorylated CREB, anti-acetyl-CoA carboxylase (ACC) and anti-phosphorylated ACC antibodies were purchased from Cell Signaling Technology (Danvers, MA, USA). The anti-FGF21 antibody was purchased from ImmunoDiagnostics Limited (Sha Tin, Hong Kong) and the anti-β-ACTIN antibody was purchased from ProteinTech Group Inc. (Chicago, IL, USA).

Enzyme assay

The activities of protein kinase A (PKA) and phosphodiesterase (PDE) in the tissue extracts prepared as described above were determined using commercial assay kits according to the manufacturer's instructions (Enzo Life Sciences)

Insulin tolerance test

The mice were fasted for 5 h before undergoing the insulin tolerance test (ITT). The ITT was performed by administering an intraperitoneal injection of insulin (2 U/kg body weight (BW); Eli Lilly, Indianapolis, IN, USA). Glucose levels were monitored before and after the injection using blood glucose strips (Arkray, Kyoto, Japan). The area over the curve (AOC) is then developed to quantify the total decrease in blood glucose during the ITT[56].

[^{3}H]-2-deoxy-D-glucose uptake assay

The [^{3}H]-2-deoxy-D-glucose ([^{3}H]-2-DG) uptake assay was performed as described by BonDurant et al. with some modifications[30]. Briefly, mice were fasted for 5 h and intraperitoneally administered an [^{3}H]-2-DG solution containing 0.9% NaCl, 0.1 mM 2DG, and 32μCi/mL [^{3}H]-2DG (American Radiolabeled Chemicals, Inc., Saint Louis, MO, USA) at 10 μL/g BW with or without insulin (2 U/kg BW). After 90 min, the eWAT and the gastrocnemius were harvested, lysed in 1 N NaOH at 80 °C for 30 min, and neutralized with 12 N HCl. The samples were separated into two aliquots and five volumes of either 6% perchloric acid (i) or Somogyi buffer containing an equal volume of 0.3 N $Ba(OH)_2$ and 0.3 N $ZnSO_4$ (ii) were added. The resulting precipitate was removed by centrifugation, and the radioactivity in the supernatant was measured using a liquid scintillation counter (TRI-CARB 4810 TR; PerkinElmer Life Sciences, Inc., Boston, MA, USA). The radioactivity, indicative of the amount of [^{3}H]-2-DG uptake in each tissue sample, was determined by subtracting the measurement for (ii) from the measurement for (i) and dividing it by the tissue weight.

RNA isolation and reverse transcription quantitative polymerase chain reaction

Total RNA was extracted from the eWAT using RNA isoPlus (Takara Co., Ltd., Otsu, Japan). cDNA was synthesized from the total RNA (1.0 μg) using a reverse transcriptase (Toyobo Co., Ltd., Osaka, Japan), and cDNA was amplified using an AriaMx Realtime PCR System (Agilent Genomics, Santa Clara, CA, USA) using GoTaq qPCR Master Mix (Promega, Madison, WI, USA). The mRNA expression levels were normalized to *36B4* expression levels and are presented as relative levels. The primer sequences are listed in Supplementary Table 1.

Cell culture and transfection

3T3-L1 cells, obtained from the Human Science Research Resources Bank (Osaka, Japan), were maintained in Dulbecco's modified Eagle medium (DMEM) supplemented with 10% calf serum. To induce adipocyte differentiation, the cells were grown to confluence. They were then cultured in a differentiation medium (a 3:1 mixture of DMEM and Ham's F12 medium containing 10% fetal bovine serum, 1.6 μM insulin, 0.0005% transferrin, 180 μM adenine, 20 pM triiodothyronine, 0.25 μM dexamethasone (DEX) and 500 μM isobutylmethylxanthine (IBMX)). After 48 h, the cells were cultured in a fresh differentiation medium without DEX and IBMX and maintained for the following days. For RNA interference, on day 6 after the induction of adipocyte differentiation, a stealth small interfering RNA (siRNA) duplex targeting *Nr1d1* (Mss211362, Thermo Fisher Scientific) or a negative control siRNA (112935-200, Thermo Fisher Scientific) was transfected with or without pcDNA3.1 (+) empty vector and pcDNA3.1 *Arntl* expression vector using Lipofectamine 2000 according to the manufacturer's instructions (Thermo Fisher Scientific). The medium was replaced with fresh differentiation medium 24 h after transfection and the cells were then cultured for an additional 24 h.

Chromatin immunoprecipitation

The chromatin immunoprecipitation (ChIP) assay was performed as previously described[57], with modifications for the eWAT. Briefly, the eWAT from 12-week-old *Arntl*$^{flox/flox}$ and AAKO mice was harvested at zeitgeber time (ZT) 10 and ZT22, cross-linked in 1% formaldehyde, and lysed. The tissue extracts were then subjected to immunoprecipitation using an anti-REV-ERBα antibody (Cell Signaling Technology). Parallel samples were incubated with non-immune IgG (Fujifilm Wako Pure Chemical) as the negative control. The DNA region was amplified and quantified using quantitative polymerase chain reaction (qPCR). Data are expressed as the fold enrichment of IgG.

The following PCR primers were used:

Arntl retinoic acid receptor-related orphan receptor-responsive element (RORE) -53/ + 31 (forward: 5'-GCCAATTCACATTTCAACCA-3', reverse: 5'- GACACAAGGCAGCATTTCAA-3'),

Fgf21 ROREs -325/-55 (forward: 5'-ACTAAGGTGAAGATCCCA ACCTCC-3', reverse: 5'- CCCCACTCCTGACGCGTGATATTT-3'), and

Fgf21 non-RORE -3793/-3733 (forward: 5'-GTTGAGCGGGCTCC GTATAG-3', reverse: 5'- GATAGTCTCCACGACGCACA-3').

Statistical analysis

Statistical analyses were performed using GraphPad Prism 6 software (GraphPad Software, La Jolla, CA, USA). Data are expressed as the mean and standard deviation (SD). Differences between two groups were determined using an unpaired Student's *t*-test with Welch's correction. Two-way analysis of variance (ANOVA) was performed on the genotype and one more condition experiment using Bonferroni's or Tukey's post hoc test. Circadian rhythmicity was assessed using the CircWave software[58]. Statistically significance was set at $P < 0.05$.

Data Availability

The datasets used and analyzed during the current study available from the corresponding author on reasonable request.

Abbreviations:

2-DG	2-deoxy-D-glucose
AAKO	Adipocyte-specific Arntl knockout
ACC	Acetyl CoA carboxylase
Adipoq	Adiponectin
AdKO	Adipocyte-specific Arntl and Fgf21 double knockout
Arntl	Aryl hydrocarbon receptor nuclear translocator like 1
ANOVA	Analysis of variance
BMAL1	Brain and muscle arnt-like protein 1
BW	Body weight
ChIP	Chromatin immunoprecipitation
CLOCK	Circadian locomotor output cycles kaput
Cry	Cryptochrome
DEX	Dexamethasone
DMEM	Dulbecco's modified Eagle medium
eWAT	Epididymal white adipose tissue
FGF21	Fibroblast growth factor 21
H&E	Hematoxylin and eosin
HSL	Hormone sensitive lipase
IBMX	Isobutylmethylxanthine
ITT	Insulin tolerance test
KO	Knock out
LAKO	Liver-specific Arntl KO mice
NEFA	Non-esterified fatty acids
PDE	Phosphodiesterase
Per	Period
PKA	Protein kinase A
REV-ERBα	Reverse orientation the c-erbA-1 gene alpha
RORE	Retinoic acid receptor-related orphan receptor-responsive elements
RORα	Retinoid-related orphan receptor alpha
RQ	Respiratory quotient
qPCR	Quantitative PCR
SD	Standard deviation
SDS-PAGE	Sodium dodecyl sulfate-polyacrylamide gel electrophoresis
TG	Triglyceride
VO_2	Oxygen consumption
ZT	Zeitgeber time

Received: 31 August 2024; Accepted: 16 January 2025;
Published online: 03 February 2025

References

1. Lowrey, P. L. & Takahashi, J. S. Genetics of circadian rhythms in mammalian model organisms. *Adv. Genet.* **74**, 175–230 (2011).
2. Hao, H., Allen, D. L. & Hardin, P. E. A circadian enhancer mediates PER-dependent mRNA cycling in Drosophila melanogaster. *Mol. Cell Biol.* **17**, 3687–3693 (1997).
3. Hogenesch, J. B., Gu, Y.-Z., Jain, S. & Bradfield, C. A. The basic-helix-loop-helix-PAS orphan MOP3 forms transcriptionally active complexes with circadian and hypoxia factors. *Proc. Natl Acad. Sci. USA* **95**, 5474–5479 (1998).
4. Gekakis, N. et al. Role of the CLOCK protein in the mammalian circadian mechanism. *Science* **280**, 1564–1569 (1998).
5. Takahata, S. et al. Transcriptionally active heterodimer formation of an Arnt-like PAS Protein, Arnt3, with HIF-1a, HLF, and Clock. *Biochem. Biophys. Res. Commun.* **248**, 789–794 (1998).
6. Kume, K. et al. mCRY1 and mCRY2 are essential components of the negative limb of the circadian clock feedback loop. *Cell* **98**, 193–205 (1999).
7. Zhang, R., Lahens, N. F., Balance, H. I., Hughes, M. E. & Hogenesch, J. B. A circadian gene expression atlas in mammals: Implications for biology and medicine. *Proc. Natl Acad. Sci. USA* **111**, 16219–16224 (2014).

8. Koike, N. et al. Transcriptional architecture and chromatin landscape of the core circadian clock in mammals. *Science* **338**, 349–354 (2012).
9. Rey, G. et al. Genome-wide and phase-specific DNA-binding rhythms of BMAL1 control circadian output functions in mouse liver. *PLoS Biol*. **9**, e1000595 https://doi.org/10.1371/journal.pbio.1000595 (2011).
10. Bunger, M. K. et al. Mop3 is an essential component of the master circadian pacemaker in mammals. *Cell* **103**, 1009–1017 (2000).
11. Kondratov, R. V., Kondratova, A. A., Gorbacheva, V. Y., Vykhovanets, O. V. & Antoch, M. P. Early aging and age-related pathologies in mice deficient in BMAL1, the core component of the circadian clock. *Genes Dev.* **20**, 1868–1873 (2006).
12. Shimba, S. et al. Deficient of a clock gene, brain and muscle arnt-like protein-1 (BMAL1), induces dyslipidemia and ectopic fat formation. *PLoS ONE* **6**, e25231 https://doi.org/10.1371/journal.pone.0025231 (2011).
13. Turek, F. W. et al. Obesity and metabolic syndrome in circadian clock mutant mice. *Science* **308**, 1043–1045 (2005).
14. Covassin, N., Singh, P. & Somers, V. K. Keeping up with the clock: circadian disruption and obesity risk. *Hypertension* **68**, 1081–1090 (2016).
15. Eckel-Mahan, K. & Sassone-Corsi, P. Metabolism and the circadian clock converge. *Physiol. Rev.* **93**, 107–135 (2013).
16. Gómez-Abellán, P., Hernández-Morante, J. J., Luján, J. A., Madrid, J. A. & Garaulet, M. Clock genes are implicated in the human metabolic syndrome. *Int. J. obesity* **32**, 121–128 (2008).
17. Maury, E., Navez, B. & Brichard, S. M. Circadian clock dysfunction in human omental fat links obesity to metabolic inflammation. *Nat. Commun*. **12**, 2388 (2021).
18. Ribas-Latre, A. et al. Cellular and physiological circadian mechanisms drive diurnal cell proliferation and expansion of white adipose tissue. *Nat. Commun.* **12**, 3482 (2021).
19. Wang, S. et al. PPAR-γ integrates obesity and adipocyte clock through epigenetic regulation of Bmal1. *Theranostics* **12**, 1589–1606 (2022).
20. Milagro, F. I. et al. CLOCK, PER2 and BMAL1 DNA methylation: association with obesity and metabolic syndrome characteristics and monounsaturated fat intake. *Chronobiol. Int.* **29**, 1180–1194 (2012).
21. Samblas, M., Milagro, F. I., Gómez-Abellán, P., Martínez, J. A. & Garaulet, M. Methylation on the circadian gene BMAL1 is associated with the effects of a weight loss intervention on serum lipid levels. *J. Biol. Rhythms* **31**, 308–317 (2016).
22. Fang, Z. et al. Sex-specific genetic association of brain and muscle Arnt-like protein-1 (BMAL1) and obesity in Chinese youth. *Obes. Res. Clin. Pract.* **16**, 464–469 (2022).
23. Shostak, A., Meyer-Kovac, J. & Oster, H. Circadian regulation of lipid mobilization in white adipose tissues. *Diabetes* **62**, 2195–2203 (2013).
24. Paschos, G. K. et al. Obesity in mice with adipocyte-specific deletion of clock component Arntl. *Nat. Med.* **18**, 1768–1777 (2012).
25. Garton, A. J. et al. Phosphorylation of bovine hormone-sensitive lipase by the AMP-activated protein kinase. *Eur. J. Biochem.* **179**, 249–254 (1989).
26. Garton, A. J. & Yeaman, S. J. Identification and role of the basal phosphorylation site on hormone-sensitive lipase. *Eur. J. Biochem.* **191**, 245–250 (1990).
27. Anthonsen, M. W., Rönnstrand, L., Wernstedt, C., Degerman, E. & Holm, C. Identification of novel phosphorylation sites in hormone-sensitive lipase that are phosphorylated in response to isoproterenol and govern activation properties in vitro. *J. Biol. Chem.* **273**, 215–221 (1998).
28. Degerman, E. et al. Phosphorylation and activation of hormone-sensitive adipocyte phosphodiesterase type 3B. *Methods* **14**, 43–53 (1998).
29. Kitamura, T. et al. Insulin-induced phosphorylation and activation of cyclic nucleotide phosphodiesterase 3B by the serine-threonine kinase Akt. *Mol. Cell Biol.* **19**, 6286–6296 (1999).
30. BonDurant, L. D. et al. FGF21 regulates metabolism through adipose-dependent and -independent mechanisms. *Cell Metab.* **25**, 935–944.e4 (2017).
31. Preitner, N. et al. The orphan nuclear receptor REV-ERBα controls circadian transcription within the positive limb of the mammalian circadian oscillator. *Cell* **110**, 251–260 (2002).
32. Ueda, H. R. et al. A transcription factor response element for gene expression during circadian night. *Nature* **418**, 534–539 (2002).
33. Lazar, M. A., Hodin, R. A., Darling, D. S. & Chin, W. W. A novel member of the thyroid/steroid hormone receptor family is encoded by the opposite strand of the rat c-erbAα transcriptional unit. *Mol. Cell Biol.* **9**, 1128–1136 (1989).
34. Miyajima, N. et al. Two erbA homologs encoding proteins with different T3 binding capacities are transcribed from opposite DNA strands of the same genetic locus. *Cell* **57**, 31–39 (1989).
35. Tong, X. et al. Transcriptional repressor E4-binding protein 4 (E4BP4) regulates metabolic hormone fibroblast growth factor 21 (FGF21) during circadian cycles and feeding. *J. Biol. Chem.* **285**, 36401–36409 (2010).
36. Wang, Y., Solt, L. A. & Burris, T. P. Regulation of FGF21 expression and secretion by retinoic acid receptor-related orphan receptor. *J. Biol. Chem.* **285**, 15668–15673 (2010).
37. Estall, J. L. et al. PGC-1α negatively regulates hepatic FGF21 expression by modulating the heme/Rev-Erbα axis. *Proc. Natl Acad. Sci. USA* **106**, 22510–22515 (2009).
38. Chavan, R. et al. REV-ERBα regulates Fgf21 expression in the liver via hepatic nuclear factor 6. *Biol. Open* **6**, 1–7 (2017).
39. Loten, E. G. & Sneyd, J. G. An effect of insulin on adipose-tissue adenosine 3':5'-cyclic monophosphate phosphodiesterase. *Biochem. J.* **120**, 187–193 (1970).
40. Manganiello, V. & Vaughan, M. An effect of insulin on cyclic adenosine 3′:5′-monophosphate phosphodiesterase activity in fat cells. *J. Biol. Chem.* **248**, 7164–7170 (1973).
41. Zinman, B. & Hollenberg, C. H. Effect of insulin and lipolytic agents on rat adipocyte low Km cyclic adenosine 3′:5′-monophosphate phosphodiesterase. *J. Biol. Chem.* **249**, 2182–2187 (1974).
42. Sakai, T., Thompson, W. J., Lavis, V. R. & Williams, R. H. Cyclic nucleotide phosphodiesterase activities from isolated fat cells: Correlation of subcellular distribution with effects of nucleotides and insulin. *Arch. Biochem. Biophys.* **162**, 331–339 (1974).
43. Markan, K. R. et al. Circulating FGF21 is liver derived and enhances glucose uptake during refeeding and overfeeding. *Diabetes* **63**, 4057–4063 (2014).
44. Staiger, H., Keuper, M., Berti, L., de Angelis, M. H. & Häring, H.-U. Fibroblast Growth Factor 21—Metabolic role in mice and men. *Endocr. Rev* **38**, 468–488 (2017).
45. Sato, T. K. et al. A functional genomics strategy reveals rora as a component of the mammalian circadian clock. *Neuron* **43**, 527–537 (2004).
46. Kettner, N. M. et al. Circadian dysfunction induces leptin resistance in mice. *Cell Metab.* **22**, 448–459 (2015).
47. Urs, S., Harrington, A., Liaw, L. & Small, D. Selective expression of an aP2/Fatty Acid Binding Protein4-Cre transgene in non-adipogenic tissues during embryonic development. *Transgenic Res.* **15**, 647–653 (2006).
48. Martens, K., Bottelbergs, A. & Baes, M. Ectopic recombination in the central and peripheral nervous system by aP2/FABP4-Cre mice: implications for metabolism research. *FEBS Lett.* **584**, 1054–1058 (2010).
49. Heffner, C. S. et al. Supporting conditional mouse mutagenesis with a comprehensive cre characterization resource. *Nat. Commun*. **3**, 1218 https://doi.org/10.1038/ncomms2186 (2012).
50. Nakagomi, A. et al. Role of the central nervous system and adipose tissue BDNF/TrkB axes in metabolic regulation. *NPJ Aging Mech. Dis.* **1**, 1–11 (2015).
51. Eguchi, J. et al. Transcriptional control of adipose lipid handling by IRF4. *Cell Metab.* **13**, 249–259 (2011).

52. Lee, K. Y. et al. Lessons on conditional gene targeting in mouse adipose tissue. *Diabetes* **62**, 864–874 (2013).
53. Zhou, B. et al. CLOCK/BMAL1 regulates circadian change of mouse hepatic insulin sensitivity by SIRT1. *Hepatology* **59**, 2196–2206 (2014).
54. Zhang, D. et al. Liver clock protein BMAL1 promotes de novo lipogenesis through insulin-mTORC2-AKT signaling. *J. Biol. Chem.* **289**, 25925–25935 (2014).
55. Jager, J. F. et al. The nuclear receptor Rev-erb alpha regulates adipose tissue-specific FGF21 signaling. *J. Biol. Chem.* **291**, 10867–10875 (2016).
56. Virtue, S. & Vidal-Puig, A. GTTs and ITTs in mice: simple tests, complex answers. *Nat. Metab.* **3**, 883–886 (2021).
57. Wada, T., Sunaga, H., Ohkawara, R. & Shimba, S. AhR modulates NADPH oxidase activity via direct transcriptional regulation of p40phox expression. *Mol. Pharmacol.* **83**, 1133–1140 (2013).
58. Oster, H. et al. The circadian rhythm of glucocorticoids is regulated by a gating mechanism residing in the adrenal cortical clock. *Cell Metab.* **4**, 163–173 (2006).

Acknowledgements

This work is in part supported by MEXT/JSPS KAKENHI (Grant Number 17K08291, 17K08392, 20K07020, 21K06536: S.S. and T.W.). The Science Research Promotion Fund from The Promotion and Mutual Aid Corporation for Private Schools of Japan (S.S. and T.W.), "Private University Research Branding Project" from MEXT (S.S.), A grant for cooperative research in the School of Pharmacy, Nihon University (S.S. and T.W.), Multidisciplinary Research Grant from Nihon University (S.S. and T.W.), A grant to encourage and promote research project in the School of Pharmacy, Nihon University (T.W.).

Author contributions

Participated in research design, H.I., S.K., T.W., and S.S. Conducted experiments, H.I., S.K., T.W., and S.S.Contributed new reagents or analytic tools, H.I., S.K., T.W., and S.S.Performed data analysis, H.I., S.K., T.W., and S.S. Wrote or contributed to the writing of the manuscript, H.I., T.W., and S.S.

Competing interests

The authors declare no competing interests.

Additional information

Supplementary information The online version contains supplementary material available at https://doi.org/10.1038/s44323-025-00023-7.

Correspondence and requests for materials should be addressed to Shigeki Shimba.